HHS Public Access

Author manuscript

Adv Funct Mater. Author manuscript; available in PMC 2021 August 04.

Published in final edited form as:

Adv Funct Mater. 2020 March 24; 30(13): . doi:10.1002/adfm.201905544.

A Wirelessly Controlled Smart Bandage with 3D-Printed Miniaturized Needle Arrays

Hossein Derakhshandeh,
Department of Mechanical and Materials Engineering, University of Nebraska, Lincoln, NE 68588, USA

Fariba Aghabaglou,
Department of Mechanical and Materials Engineering, University of Nebraska, Lincoln, NE 68588, USA

Alec McCarthy,
Department of Mechanical and Materials Engineering, University of Nebraska, Lincoln, NE 68588, USA

Azadeh Mostafavi,
Department of Mechanical and Materials Engineering, University of Nebraska, Lincoln, NE 68588, USA

Chris Wiseman,
Department of Mechanical and Materials Engineering, University of Nebraska, Lincoln, NE 68588, USA

Zack Bonick,
Department of Mechanical and Materials Engineering, University of Nebraska, Lincoln, NE 68588, USA

Ian Ghanavati,
Department of Mechanical and Materials Engineering, University of Nebraska, Lincoln, NE 68588, USA

Seth Harris,
Veterinary Diagnostic Center, School of Veterinary Medicine and Biomedical Sciences, University of Nebraska-Lincoln Lincoln, NE 68583, USA

Craig Kreikemeier-Bower,
Institutional Animal Care Program, University of Nebraska–Lincoln, Lincoln, NE 68583, USA

Seyed Masoud Moosavi Basri,

atamayol@uchc.edu.

Supporting Information

Supporting Information is available from the Wiley Online Library or from the author.

Conflict of Interest

The authors declare no conflict of interest.

The ORCID identification number(s) for the author(s) of this article can be found under https://doi.org/10.1002/adfm.201905544.

Department of Biomedical Engineering, American University of Sharjah, Sharjah 26666, United Arab Emirates

Jordan Rosenbohm,
Department of Mechanical and Materials Engineering, University of Nebraska, Lincoln, NE 68588, USA

Ruiguo Yang,
Department of Mechanical and Materials Engineering, University of Nebraska, Lincoln, NE 68588, USA

Regenerative Medicine Program, University of Nebraska Medical Center, Omaha, NE 68198, USA

Pooria Mostafalu,
Department of Medicine, Brigham and Women's Hospital, Harvard Medical School, Boston, MA 02139, USA

Dennis Orgill,
Division of Plastic Surgery, Brigham and Women's Hospital, Harvard Medical School, Boston, MA 02115, USA

Ali Tamayol
Department of Mechanical and Materials Engineering, University of Nebraska, Lincoln, NE 68588, USA

Regenerative Medicine Program, University of Nebraska Medical Center, Omaha, NE 68198, USA

Department of Biomedical Engineering, University of Connecticut Health Center, Farmington, CT 06030, USA

Abstract

Chronic wounds are one of the most devastating complications of diabetes and are the leading cause of nontraumatic limb amputation. Despite the progress in identifying factors and promising in vitro results for the treatment of chronic wounds, their clinical translation is limited. Given the range of disruptive processes necessary for wound healing, different pharmacological agents are needed at different stages of tissue regeneration. This requires the development of wearable devices that can deliver agents to critical layers of the wound bed in a minimally invasive fashion. Here, for the first time, a programmable platform is engineered that is capable of actively delivering a variety of drugs with independent temporal profiles through miniaturized needles into deeper layers of the wound bed. The delivery of vascular endothelial growth factor (VEGF) through the miniaturized needle arrays demonstrates that, in addition to the selection of suitable therapeutics, the delivery method and their spatial distribution within the wound bed is equally important. Administration of VEGF to chronic dermal wounds of diabetic mice using the programmable platform shows a significant increase in wound closure, re-epithelialization, angiogenesis, and hair growth when compared to standard topical delivery of therapeutics.

Keywords

3D-printed needles; active drug delivery; chronic wounds; smart bandages

1. Introduction

Plaguing an estimated 4.5 million Americans each year,[1] chronic wounds are typically defined as wounds that fail to self-heal after 3 months and can often persist for over a year.[2] While there are many reasons for the occurrence of chronic wounds, they are the most commonly seen as a devastating side effect of type II diabetes. Due to the increases in aging population, obesity, and type II diabetes, chronic diabetic wound occurrences have increased markedly.[3] Additionally, chronic wounds are the leading cause of nontraumatic limb amputation.[4]

In chronic wounds, the highly orchestrated cascade of physiological processes leading to wound healing is typically disrupted, leading to extreme hypoxia from the lack of angiogenesis, immune-modulated hyper inflammation, biofilm formation, and bacterial infection.[5] It should be noted that individual wound pathophysiology may differ, and each wound could have its own characteristics. As a result, it is challenging to introduce a unique treatment that is applicable to all types of wounds. However, most complications result from the lack of vascularization, which will result in common themes seen among chronic wounds such as the formation of necrotic tissue, significant inflammation, and exudate production.[4b,6] Impaired angiogenesis significantly limits the availability of vital nutrients, oxygen, immune cells, and epithelial cells at the injury site. Without oxygen and nutrients, areas of necrotic tissue grow, which are conducive to the growth of biofilms.[7] The formed biofilms on top of the wound bed are resistant to treatment by topical and systemic delivery of antibiotics.[5]

There have been numerous research and clinical efforts testing different factors, peptides, or their combination for fueling various physiological processes leading to the healing of chronic wounds.[4a,8] Due to the accessibility of cutaneous wounds, biological factors are usually delivered topically using dressings, ointments, or scaffolds.[9] Antibiotics have been delivered both systemically and topically.[4b] In addition, different biological factors are required at various stages of healing.[4b,10] Therefore, novel, personalized dressings that can be programmed to control the temporal delivery rate of various therapeutics are expected to improve the healing of chronic wounds.[11] There have been a number of advanced bandages that can predict the pathophysiological conditions of the wound and actively deliver drugs.[10,12] While these platforms and the newly developed therapeutics have generated significant promise in vitro, they fail to facilitate healing in clinical trials. One overlooked criterion is the importance of the point of delivery on the effectiveness of therapeutics in wound healing. In this study, for the first time, we shed light on the important role of the delivery point in inducing wound healing. Chronic wounds are typically covered by a crust and a layer of necrotic tissue, with the live tissue located below these layers.[5a] Such wounds are also exuding which can wash out the topically delivered therapeutics or deactivate them due to the presence of various enzymes and proteins. Overall, these

conditions are expected to reduce the bioavailability of drugs in the healing tissue. We explored two hypotheses in this study. First, developing a device allowing temporal control over the release kinetics of various drugs could be a strong tool in clinical practice. Second, shortening the traveling distance of therapeutics by direct delivery of drugs into the live tissues could improve their effectiveness.

Here, we report an individualized bandage for treating chronic diabetic wounds. This wearable and programmable bandage is equipped with polymeric miniaturized needle arrays (MNAs) for delivering vital pharmacological agents and growth factors into the deeper layers of the wound bed. Compared with topical administration of drugs, this innovative method proved to be more effective in promoting re-epithelialization and angiogenesis, leading to wound closure and hair growth. Further, the MNAs used in this study are minimally invasive and thereby induce minimal pain and inflammation compared to other invasive methods. Ultimately, our programmable bandage allows physicians to remotely administer therapeutics as needed. The in vitro experiments suggested the importance of the MNA-based delivery systems. These results were further confirmed in a full thickness diabetic wound model.

2. Results and Discussions

The treatment of chronic wounds is a major medical challenge.[4b] Smart systems have been developed that allow active control over drug release or even enable active control of drug release in response to changes in the wound environment.[10,13] However, most of the existing devices have undesirable drug release. The unwanted release of drugs such as antibiotics, anti-inflammatory compounds, and biological factors could negatively impact wound healing. For example, the unwanted release of antibiotics can lead to the development of resistance in colonized bacteria, complicating the treatment of potential infections.[14] We hypothesized that a system enabling precise control over the delivery of therapeutics already loaded into the bandage can serve as a strong tool in clinical practice. Such capability does not exist in any existing bandages. Also, almost all the current methods and systems used for controlling drug release in the treatment of wound care are designed for topical delivery of drugs.[7,15] This is due to the ease-of-access to the wound site, which allows for the localized delivery of therapeutics. Such systems disregard the pathophysiology of chronic wounds, which is an avascular or not sufficiently vascularized tissue, covered by necrotic tissue and a crust.[4b] In addition, wound exudates rich with various proteins, inflammatory cytokines, and even pathogens are typically flowing from the inner layers toward the wound surface. These exudates can deactivate and wash away a significant portion of the topically delivered drugs before they even reach the targeted cells. Therefore, we also hypothesized that a bandage capable of delivery of various drugs or biological factors transdermally to deeper layers of the wound bed could significantly improve the healing rate and reduce the healing time. To test our two hypotheses mentioned above, a programmable smart bandage was designed that utilized hollow MNAs to bypass the wound crust and the necrotic tissue and actively deliver therapeutics to the deeper layers of the wound bed. MNAs are categorized as minimally invasive delivery tools and are used for the transdermal delivery of therapeutics.[16]

Active pumping remains one of the most accurate methods for precisely controlling the delivery rate of drug solutions. Therefore, the platform utilized two miniaturized peristaltic pumps that could manipulate minute amounts of two different drugs with independent dosages. A conceptual schematic of the designed platform is shown in Figure 1A. Figure 1B presents the prototype of the smart bandage used in this study.

Recent advances in 3D printing have facilitated the fabrication of miniaturized structures with a suitable resolution without the need for sophisticated cleanroom microfabrication processes.[17] In this study, we used a fused deposition modeling (FDM) 3D printer to print hollow MNAs out of a biocompatible resin. The 3D printer was operated by printing support materials to fabricate the high aspect ratio MNAs. The support material of 3D printing is a gel-like soluble material for upholding the overhangs and helps for printing small cavities. The support material is subsequently removed by dissolving in NaOH solution (Figure 2A). This process allows us to fabricate MNAs with different needle spacings (1.5–3 mm), needle lengths (0.8–3 mm), base sizes (0.5–1.5 mm), and opening diameters (0.2–0.5 mm). A length of ≈2 mm was selected for MNAs to pass through the crust and part of the necrotic tissue, allowing drug delivery to the deeper layers of the wound. The thickness of the necrotic tissue depends on the type, stage, and pathophysiology of the wound. Our hypothesis was that delivery of compounds within or under wound crust and necrotic tissue should improve the therapy outcome. The reason for choosing a length of 2 mm was based on the thickness of the dermis and the epidermis in human skin, which is reported to be in the range of 0.5–2 mm.[18] These MNAs are expected to reach nerve termini in healthy populations. However, noting the fact that patients with diabetic ulcers are typically suffering from neuropathy and lack of sensation in their limbs, MNAs insertion will not cause any pain in patients.[19] The designed MNAs are capable of infusing drugs with a controlled distribution., which is not easy to achieve with hypodermic needles because they are too long and are only able to target a single point. In this study we utilized MNAs to uniformly distribute the therapeutic compounds throughout the tissue in desired depth. A representative computer model and a micrograph of fabricated MNAs are shown in Figure 2A,B. The 3D-printed MNAs were smooth and sharp enough to penetrate wounded skin (Figure 2C).

Another interesting aspect of the multimaterial 3D printing was the possibility of printing MNAs with rigid resin tips on a flexible polymeric substrate (Figure 2D). For this reason, needles were printed from a hard resin (Vero Clear, Stratasys, USA), while the backing was printed from another flexible resin (Tango Black, Stratasys, USA). In a previous study, the response of different cells including skeletal muscle (C2C12), neuronal (SH-SY5Y), and hepatic (HepG2) to 3D-printed polymers (including Vero Clear) was already assessed.[20] In this study, the biocompatibility of the resin-based MNAs was assessed by interfacing human umbilical vein cells (HUVECs) with MNAs. For visualization purposes, HUVECs were cultured directly on MNAs and after 1 day their viability was assessed by performing a live/dead assay in which the live cells appear in green, while the dead cells appear in red (Figure S1, Supporting Information). To assess the potential effects of MNAs on cellular viability and proliferation, HUVECs were cultured in multiwell plates and MNAs were placed in their culture media. The metabolic activity of the cells was then measured using a PrestoBlue assay. The assay showed that over the course of a 3 day culture, considering one-

way ANOVA analysis on the result of days 1 and 3, the *P*-values were found to be 0.5470 and 0.2346, respectively, and no statistically significant difference in cell proliferation was observed between the HUVECs cultured on MNAs and those cultured in multiwell plates as positive control (Figure S2, Supporting Information). The duration of the experiments was selected based on the intended lifespan of the fabricated bandage. One important factor in the use of MNAs is understanding their degradation rate in wound conditions. To assess this, MNAs were placed in exudate-mimicking solutions and their mass was measured over a period of 3 days. No significant change in their mass was observed in the MNAs (Figure S3, Supporting Information), suggesting an erosion resistivity of the selected materials.

The mechanical properties of MNAs play a key role in their successful utilization. For example, breakage of the needles during their use can cause inflammation and lead to further complications, negatively impacting the healing process. The mechanical properties of the MNAs under compressive loads were assessed by a mechanical tester. In this case, a maximum force of 200 N was applied and the deformation of the MNAs was measured as a function of the applied force. As shown in Figure 2E and Figure S4 (Supporting Information), the MNAs did not break and were only bent under a compressive force of ≈78 N. A similar test was conducted to assess the penetration and retraction force of the MNAs into and out of the pig skin (Figure S5, Supporting Information). No deformation or breakage were observed upon penetration and removal from the pig skin (Figure 2F). Results showed that the majority of the MNAs penetrated fresh pig skin with less than 2 N of force and full penetration was achieved with about 7 N. The pull-out force for the MNAs was measured to be about 2 N. The trace of full penetration of colored MNAs can be seen on the pig skin by red dots (Figure 2G). It should be noted that the overall force for penetrating the whole patch depends on the number of islands. An adhesive tape on the back of the bandage can be used to keep the bandage in place once the MNAs are manually inserted.

Since some drugs may react with one another, two sets of microchannel arrays, micropumps, and drug reservoirs were utilized to enable the independent handling of solutions. To ensure the flexibility of the bandage, microchannels were fabricated in a polydimethylsiloxane (PDMS) layer with a thickness of ≈1.5 mm. The end of the microchannels was then connected to MNA islands with a footprint of 10 mm × 10 mm (Figure 3A). The use of separated MNA islands further improved the flexibility of the bandage and the uniformity of drug distribution across the wound area. PDMS was used due to its flexibility, low protein adsorption, biocompatibility, and oxygen permeability.[21] The transparency of the bandage can also facilitate the visual inspection of the wound without the bandage removal. To properly bond the MNA islands to the PDMS substrate, we developed a protocol which is shown in Figure S6 (Supporting Information). The bonding strength between the 3D-printed resin and the PDMS substrate was measured using a peel-off test. The results suggested an average bonding strength of 237 kPa (Figure 3B,C) for the partial detachment of resin from the PDMS substrate (Figure S7, Supporting Information).

To form a fully integrated bandage, peristaltic micropumps (Clark Solutions, MA) were utilized to suffuse the drug solutions into the microchannel arrays and then through the MNA islands. To reduce the bandage operating cost and keep it flexible and light, it was designed with two modules, a disposable module with the MNA islands and microchannel

arrays, and a reusable module, which housed the drug reservoirs, micropumps, power source, and electrical circuitry (Figure 3E). The two modules were connected using two flexible silicon tubes (Figure 3F). The micropumps were controlled by applying a pulse width modulated digital signal from a microcontroller. The platform could be interfaced with smartphones through Bluetooth. An app was designed to regulate the remote programming of the bandage. The relationship between the applied voltage and the achieved flow rates was determined and is presented in Figure 3G. The minimum threshold of the pumps was determined to be 0.5 V, which resulted in the flow rate of 43.6 μL min^{-1}. The data in Figure 3G was used to generate calibration curves to program the app and precisely control the flow rate. The reproducibility of the generated flow rates was assessed over an hour.

In addition, to test the micropump's response to dynamic actuation and having control over time and dosage of drug delivery, the drivers were programmed to periodically apply a constant maximum voltage of 3.0 V. The response of the micropumps to dynamic actuation is shown in Figure 3H,I for periodic delivery of aqueous solutions. As the voltage value reached zero, the pumping stopped. It can be seen that the pumping process stops as soon as the applied voltage is zeroed. This system can deliver up to two types of drugs with independent dosage. As an example, we set each of the micropumps to operate simultaneously with different delivery scenarios (Figure S8, Supporting Information). As expected, pump 1 (Figure 3H) delivered a dosage of 200 μL every 6 min, while pump 2 (Figure 3I) delivered 400 μL every 10 min based on an example scenario which was set with the wireless app (Figure S8, Supporting Information). It should be noted that the micropumps can also be set to work continuously at desired flow rate. Figure S9 (Supporting Information) shows continuous delivery at the maximum (478 μL min^{-1}) and minimum (44 μL min^{-1}) flow rate for micropumps 1 and 2, respectively. The flow rate that can be achieved using the micropumps was in a range comparable to some of the existing medical devices. For instance, "Medfusion 3500 Syringe Pump" is an intuitive system designed for transdermal drug delivery for clinical settings with a flow rate range of 0.16–18833 μL min^{-1}. Once the system was characterized, the efficiency of the bandage in drug delivery was evaluated. Initially, the potential drug adsorption into the engineered bandage was tested. For this reason, bovine serum albumin (BSA) and cefazolin with the concentrations of 54 and 16 μg mL^{-1} in phosphate buffered saline (PBS) were loaded into the bandage as model drugs, respectively. The solution was then collected at different time points after perfusion through the MNAs and the concentration of the drugs was determined using a total protein assay (for BSA) and UV–vis spectrophotometry (for cefazolin). As shown in Figure 4A,B, the temporal changes in the drug concentration within the perfused solution was not statistically significant, suggesting low adsorption of proteins and antibiotics. To assess the importance of the MNAs for the treatment of chronic wounds, we developed an in vitro model resembling the crust and necrotic tissue covering the viable tissue (Figure 4C). The in vitro model is comprised of a cell culture insert with 3 μm pore size coated by ≈2 mm thick 3% (w/v) agarose gel; the interior of the well plate was filled with PBS representing the environment of live cells. Agarose gel has been used as a skin phantom in several studies and offers porosity and texture similar to skin.[22] To simulate topical drug delivery, 100 μL of drug solution was added on top of the agarose gel. To test the MNA-based delivery, a miniaturized bandage with a diameter of 10 mm (Figure S10, Supporting Information) was

fabricated by 3D printing and placed in the agarose gel followed by the delivery of 100 μL of the drug solution using a syringe.

Figure 4D,E represents the cumulative concentration of protein delivered over time, revealing that MNAs enabled a rapid delivery of proteins to the lower chamber representing the environment below the necrotic tissue in comparison to the drug delivered topically. The results suggest that 70% of the protein was delivered into the bottom chamber using MNAs after 180 min, while only 1% of the drug was delivered when BSA solution was added on top of the agarose gel. A similar methodology was applied for the assessment of the effectiveness of VEGF as an angiogenic factor on the culture of HUVECs in vitro. For the experiments, a 200 μm scratch was made in the confluent monolayer culture of HUVECs and VEGF was delivered. Four groups were studied, including 1) 50 ng mL^{-1} of VEGF in the culture medium (positive control), 2) no VEGF (negative control), 3) equivalent to 50 ng mL^{-1} of culture media delivered topically, and 4) equivalent to 50 ng mL^{-1} of culture media delivered using the MNAs. VEGF was delivered once during the in vitro experiments. The data suggests that the group receiving VEGF through MNAs had a migration rate comparable to the positive control group which received VEGF in their culture medium, and 100% scratch closure was achieved in 4 h. The migration and the scratch closure rates in the group receiving VEGF topically was faster than the negative control. However, the migration rate in this group was significantly slower than the two other groups (Figure 4F,G).

Results from the in vitro study suggested the positive effect of MNAs in increasing the drug bioavailability at the site of healthy cells in the wound bed below the wound crust. To further investigate the potential benefits of MNAs in the treatment of diabetic and chronic wounds, an animal study was conducted on diabetic mice with cutaneous wounds. Homozygous mice for the diabetes spontaneous mutation (*Lepr*db) become identifiably obese around 3–4 weeks of age. Elevation of plasma insulin begins between days 10 and 14, and blood sugar levels elevate at four to eight weeks. With a delayed wound healing and an increased metabolic efficiency, this mouse strain serves as a suitable model for chronic wound research.[23] It should be noted that rodents, including mice, do not capture the wound healing mechanisms in humans. The used animal model is a well-established model widely used in literature for pilot studies of wound care products.[24] Positive results should perhaps be verified in more relevant animal models.

Animals were divided into three study groups, including 1) negative control with no treatment ($n = 4$); 2) topical group, where 100 μL of 500 ng mL^{-1} of VEGF solution was pipetted on the wound ($n = 4$); and 3) MNA group in which 100 μL of 500 ng mL^{-1} VEGF solution was delivered using MNAs over 10 min into the wound bed ($n = 5$). Needles were pushed completely into the wound bed and no leakage was observed during penetration. On day 1, all the mice received a square-shaped 1 cm × 1 cm full thickness skin cut on their dorsum. The animals were kept untreated for 5 days to allow for the formation of a wound crust. On days 5 and 7 postsurgery animals received the planned treatment. Excessive intervention with the wound bed could negatively affect the healing process and was avoided. Our hypothesis was that the localized increase in VEGF concentration for only a few days should be enough to induce sufficient angiogenesis to support the formation of new tissue. In addition, we expected that the delivery of VEGF at only two time points could be

sufficient to induce healing. No edema was observed postdelivery of VEGF as shown in Figure S12 (Supporting Information). The animals' weights were recorded periodically, and the wound area was assessed every two days and photographs were captured to investigate wound closure (Figure 5A). The wound area was measured, and the statistical analysis showed significant differences in the wound closure rate in the MNA group compared to the topical and control groups from day 13 postsurgery. On day 15, statistical analysis showed significantly different wound closure rates in animals receiving VEGF by MNAs compared to the negative control group. On days 17 and 19, the wound closure in the MNA group was significantly faster than both topical delivery and negative control groups. At day 19, the average wound size in the MNA group decreased to 0.04 cm^2 with an average of 95% closure. At the end of the 19 day study, the animals in the topical delivery group reached about 55% closure, while the negative control group showed about 40% closure. No significant difference was observed in the wound closure rate of animals that received VEGF delivery topically compared to the negative control group (Figure 5B,C).

Another important observation was the significant difference in the quality of wound healing (Figure S11, Supporting Information). In all animals receiving VEGF through MNAs, hair growth in the new tissue was observed. Typically, full thickness injuries result in scarring, which leads to the lack of hair growth. However, in the MNA group, there was scarring histologically at the edge of the wounds, but it was not visible grossly on the examination of the wounds at the end of the experiments. The observation of hair growth due to VEGF delivery might be due to better wound vascularization and in growth and differentiation of the new tissue. It should be noted that the positive role of VEGF on new hair growth has been suggested previously.[25] However, more detailed experiments are required to understand the mechanism of stimulating hair growth. Similar to many other studies, no hair growth was observed in the wound area for the animals in both topical delivery and negative control groups.

With histological evaluation, the junction of the surgical wound and adjacent skin of all treatment groups had a healing site, which was mildly to moderately thickened by granulation tissue. This junctional area of granulation tissue bordering the normal haired skin from peripheral to the wound contained entrapped pilosebaceous units. The appearance of the junctional skin was indistinguishable among all of the mice, indicating that the shrunken wounds in the MNA treated groups had followed orderly wound healing with regrowth of all dermal, follicular, and epidermal elements through nearly the entire wound site.

The evaluation of the thickness of granulation in the center of the wound showed significant increase in thickness of granulation in animals receiving VEGF via MNAs compared to topical delivery and negative control groups (Figure S13, Supporting Information). The granulation tissue within the center of the surgical wounds in the treatment groups that had not undergone healing was associated with alopecia, deposition of collagen, and neovascularization, compatible with cutaneous scarring. It should be noted that the comparison of the wound closure and formation of hair follicles in the animal group receiving VEGF through MNAs indirectly suggests the presence of enough vasculature to support the formation of new tissue.

Further evaluation of wound healing parameters was done utilizing immunofluorescence assays for CD-31 (Figure S14, Supporting Information) and MMP9 (Figure S15, Supporting Information). CD-31 is a transmembrane protein that is expressed by endothelial cells and its presence is an indicator of vascularization. When compared against both the topically treated and negative controls, the MNA group had significantly higher CD-31 expressing cells, which was expected given the thicker bed of granulation tissue at the center of the wound. MMP9 is a protease involved in degradation of the extracellular matrix. Overall, in the experimental group there was a decreased MMP9 expression in the MNA group when compared against the negative control. While not a solitary indicator of inflammation, degradation products of MMP9 can act as chemokines resulting in the attraction of leukocytes in addition to the other better characterized roles of collagen remodeling. These results expound on the histological findings that VEGF delivery though MNAs resulted in an increased wound healing due to increased vascularization and decreased MMP9 activity at the tested time point. Similar studies in future on wild-type animals and at different time points can provide more information about the range of applicability of the proposed solution and the changes in the rate of wound healing, respectively.

To date, the majority of research activities in this field have been focused on either identifying suitable compounds facilitating important physiological processes required for the healing of chronic wounds or determining the optimal temporal profile for their release. In other words, the research activities have tried to find “what” and “when” to be delivered. However, our animal data challenge the presumption that cutaneous wounds are easily accessible with drugs applied topically. We believe that for better treatment outcomes, therapies should decide about “what,” “when,” and “where”; and this “where” is supplied by innovative delivery methods such as the one proposed in the current study.

3. Conclusions

The treatment of chronic wounds has remained a major medical challenge and devices that can reduce the need for frequent visits to medical facilities while enabling the possibility of releasing different drugs independently would be valuable. One important question in wound care is if the topical delivery of drugs is suitable for the treatment of exuding chronic wounds covered with a crust and necrotic tissue. Here, we developed a programmable platform with the capability of actively controlling the release profile of multiple drugs. The platform benefits from multiple miniaturized pumps wirelessly controlled through an in-house smartphone application. All the electronics were integrated into a smartphone sized module that could be reused. To improve the bioavailability of drugs and active compounds in deeper layers of the tissue, the bandage was equipped with islands of MNAs. The effectiveness of the MNAs in transferring the active compounds through the wound crust and necrotic tissues were successfully demonstrated in vitro. The platform was then utilized for the delivery of VEGF for the treatment of 5 day old full thickness skin injuries in diabetic mice. The results showed a significant difference in wound closure and a fundamental difference in healing quality. The animals that received VEGF through the MNAs showed signs of complete healing and a lack of scar formation. Our data suggested that, in addition to the active compounds and their release profile, the point of delivery should be considered as equally important in treating chronic wounds. As a result, the use of

MNA-based patches for wound care could be an effective paradigm shift from the current methods used in clinical wound care practices.

4. Experimental Section

Materials:

and reagents including NaOH, cefazolin, (3-aminopropyl) triethoxysilane (APTES), HUVEC culture media, BCA Protein Assay kit 23225, Human VEGF 165, fetal bovine serum (FBS), Geltrex matric, and PBS were purchased from Sigma-Aldrich (MO, USA). Polydimethylsiloxane (PDMS) was purchased from Dow (MI, USA). 3D-printing resins were obtained from Stratasys (MN, USA). Recombinant mouse VEGF (VEGF 164) was purchased from Biolegend (CA, USA) and anti-CD31 antibody (ab56299), anti-MMP9 antibody (ab38898), were purchased from Abcam (Cambridge, MA). gGoat antirat IgG (H+L) secondary antibody, Alexa Fluor 488, and goat antirabbit IgG (H+L) secondary antibody, Alexa Fluor 594 were purchased from Thermo Fisher Scientific (Waltham, MA).

MNA Fabrication and Integration into the Bandage:

MNAs were fabricated using an FDM 3D printer (Objet 500 Connex3, Stratasys, USA) out of Veroclear RGD 810 (Stratasys, MN, USA). After 3D printing of the MNAs, the support material was removed using 3% (w/v) NaOH solution in an ultrasonic bath. Micromolding of PDMS was used to fabricate a flexible bandage with incorporated microchannel patterns. To permanently bond MNAs to the PDMS bandage, the pieces were silanized by APTES overnight. Both surfaces of the MNAs and bandage were then activated using a plasma cleaner (Harrick Plasma, USA) in high mode for 15 s. The samples were interfaced and kept under pressure (using a 1 lb weight) at 80 °C for 2 h to complete the bonding. The bonding strength between resin and PDMS was measured using a mechanical tester (CellScale Univert). Cubic samples of PDMS and Resin (1 cm^3) were fabricated and bonded together as described above. The force required for the detachment of the pieces were measured. The experiments were done in four replicates.

The mechanical strength of the MNAs was measured under a compressive load using the mechanical tester. MNAs were glued on the lower grip of the mechanical tester. Then, the upper jaw was brought in contact with the array and a compressive load was applied by moving the jaws at a rate of 0.092 mm s^{-1}. The experiments were done in triplicates.

The characterization of MNAs penetration through pig skin was evaluated using the mechanical tester. To this mean, MNAs were glued to the upper jaw of the mechanical tester and a 3 cm × 3 cm fresh pig skin was placed on the lower jaw. The jaws were moved until the MNAs were touching the skin and the device was run under the compression mode at a rate of 0.27 mm s^{-1}. After penetration, the samples were left at rest for 1 min and then they were retracted by running the mechanical tester under the tensile loading mode (at the same rate of insertion) to measure the pull-out force.

In order to evaluate the possible degradation of MNAs in situ, a wound exudate mimicking solution was generated according to previous studies. The solution contained 0.368 g $CaCl_2$ and 8.29 g NaCl (pH 8.2), which were dissolved into 1000 mL of distilled water and stirred

for 10 min. Twelve MNAs were prepared as previously described, rinsed with distilled water, and fully submerged in 3 mL of exudate mimicking solution at 37 °C. On days 1, 3, 5, and 7, the weight of the dry MNAs was measured to determine the rate of mass loss.

Integration of Pumps and Electronics:

An RPQ1 peristaltic micropump was chosen to precisely control drug administration given its ability to manipulate small quantities of medication. As different drugs or biological factors are needed at various stages of wound healing, the bandage was engineered to handle two different drugs independently. In order to run two pumps bidirectionally, an L293D half H-bridge (LCSC, USA) was selected as the driver. An Arduino Nano Clone (Elegoo, USA) was chosen as the microcontroller for providing 5 V logic output. To provide wireless communication, an HC-05 Bluetooth module (Hiletgo, China) was selected. A custom-built PCB (JLC PCB, USA) was used for the assembly of various components. The electronics, micropumps, and drug reservoirs were housed in a 3D-printed box (1 cm × 10 cm × 15 cm). The fabricated module was placed within an armband and was connected to the bandage with the integrated MNAs using flexible silicon micro tubing.

For maintaining proper function during administration, a simple code was written to apply a pulse width modulated signal from the Arduino pins. The code allowed the PWM value to be adjusted from 0 to 255 to simulate a variable voltage input to the pumps. This code was used to correlate the effective voltage input level to the volume of fluid dispensed. Next, an Android smartphone application was programmed using the drag and drop programming of MIT App Inventor (appinventor.mit.edu). This app allows the user to set pump dosing volume individually, either manually or on a timer, to deliver different doses at different times. This creates the opportunity to provide two different drugs to the wound. To complete the software system, an Arduino program was written to read the input transmitted from the app via Bluetooth. The program then takes the user input and converts it to milliseconds. However, the volume input was converted to the time which the pump must run at full speed to deliver the desired dose, and the calculation was done based on the data from the correlation between the voltage supplied to the micro pump and its flow rate.

Drug Delivery Characterization:

The potential protein and drug adsorption by the bandage, tubing, and MNAs were investigated by perfusing a solution with known concentrations of cefazolin salt and BSA. 150 μL of the delivered solution was collected at different time points and the concentrations of cefazolin and BSA were determined by measuring the solution absorbance for cefazolin and a BCA protein assay kit for BSA.

To develop a method for mimicking the crust and necrotic tissue covering chronic wounds, 12-well cell culture inserts were used and covered with 150 mL of 3% (w/v) agarose solution. Once the agarose gel was solidified, the insert was placed in 12-well plates, the bottom chamber was filled with 2 mL of PBS, and the active compounds were delivered. A similar technique was applied for the scratch assay with seeding HUVECs in the bottom of a chamber covered with 2 mL basal media. To mimic topical delivery, the active compounds (BSA or VEGF) were directly poured on top of the agarose gel, while in the case of MNA-

based delivery, MNAs with the diameter of 9 mm were inserted into the gel and perfusion was carried out at a rate of 7.5 μL s^{-1}.

For measuring the concentration of BSA within the solution inside the wells, 450 μL of the solution was removed and replaced with fresh PBS at each time points. The concentration of BSA was measured using a BCA total protein assay kit as per the manufacturer's protocol.

Cell Culture and In Vitro Experiments:

HUVECs were purchased from Sigma-Aldrich and were cultured in endothelial growth media (Sigma-Aldrich) and were used up to passage 6. To assess the biocompatibility of the MNAs, they were coated with Geltrex diluted 1:20 in media at 37 °C. The MNAs were seeded with about 20000 cells and after 1 day their viability was assessed using a Live/Dead Viability/Cytotoxicity Kit (Invitrogen, USA) as per the protocol recommended by the manufacturer. In brief, samples were incubated with a mixture of 2 μL mL^{-1} ethidium homodimer and 0.5 μL mL^{-1} calcein-AM in PBS for 10 min at 37 °C. The samples were imaged using a Zeiss Observer fluorescence microscope, where live cells appeared as green while the dead cells appeared in red. The effect of MNAs on cellular proliferation was assessed indirectly by measuring the metabolic activity of cells using a PrestoBlue assay (Invitrogen, USA) as per manufacturer recommended protocol. For this reason, 15 000 cells were cultured in 24-well plates and MNAs of 7 mm × 7 mm were interfaced with them. On days 1 and 3, the PrestoBlue reagent mixed with media (1:10 ratio) was added and the cultured cells were incubated for 1 h. Finally, the fluorescence intensity of the solution was measured using a Cytation 5 UV–vis spectrophotometer (Bio Tek, USA). Four samples were used, cells were seeded at the bottom of a multiwell plate and then samples were placed in their culture media to assess the effect of potentially released chemicals on cellular proliferation and the growth rate was compared to the cell cultured in multiwell plates without being interfaced with MNAs.

To assess the effectiveness of the released factors, a standard scratch assay was conducted. Wells of a 12-well plate were coated by Geltrex. After aspirating the Geltrex from wells, 30 000 cells were seeded in the wells and were cultured until a confluent monolayer was formed. The cells were cultured in basal media supplemented with 2% FBS 6 h prior to the experiments. On the day of experiments, an approximately 200 μm wide scratch was formed using a 200 μL micropipette tip. The samples were divided into 4 groups having 4 replicates for each group: 1) positive control receiving a VEGF supplement of 50 ng mL^{-1} in their culture media; 2) negative control cultured without receiving VEGF supplement; 3) MNA group receiving the same VEGF containing solution as the positive control through the MNAs placed in tissue culture inserts filled with agarose gel; 4) topical group receiving the same VEGF containing solution as the positive control by adding it on top the agarose gel within the tissue culture inserts. Fixed points of each well (two points per well) were imaged using a Nikon Ti inverted microscope after 0, 2, and 4 h post-treatment application. A total of four samples per condition were tested.

Animal Studies:

All animal procedures were reviewed and approved by the Institutional Animal Care and Use Committee (IACUC) of the University of Nebraska, Lincoln. Five week old B6.BKS(D)-Lepr^{db}/J mice were purchased from the Jackson Laboratory (Bar Harbor, ME) weighted between 34 and 43 g and accommodated in the University of Nebraska Life Science Annex animal facility for one week before the wound injury procedure. Sex-matched controlled mice were divided into three study groups including 1) negative control (no treatment) ($n = 4$), 2) test group receiving VEGF topically ($n = 4$), and 3) test group receiving VEGF through MNAs delivery ($n = 5$). Each animal received two sessions of VEGF.

On day 1, all animals were anesthetized by 5% isoflurane using an anesthesia system (VetFlo, Kent Scientific, Torrington, CT) via a nose cone. The hair on the dorsal region of the animals was shaved using an electric razor. The skin was sterilized, and a full thickness skin incision of 1 cm × 1 cm was created. All mice received Buprenorphine SR for pain relief at the time of surgery, and then the wounds were covered with a regular water proof bandage (3M Nexcare, St. Paul, MN) to mitigate wound dehydration. All mice were then placed back in separate cages individually after recovering from anesthesia. Animals were monitored for wound condition, vitals and wellbeing, and weight gain/loss trends daily.

To simulate the real wound conditions covered by crust and necrotic tissues, treatments started on day 5, by which time a complete crust was formed on the wounds. Murine VEGF was dissolved in PBS (phosphate buffered saline) containing 0.1% (w/v) BSA at a concentration of 500 ng mL^{-1} and used as an animal vascular permeability factor. In topical delivery group, 100 μL of the solution was poured topically using a pipette on the top of the wound and the animals were let to sit for about 10 min, after which the wound was covered by a fresh dressing. In MNAs delivery group, 100 μL of the solution was gradually delivered using the MNAs and after 10 min, the MNAs were removed and the wound was covered by a fresh dressing. Animals of negative control received no treatment. A similar procedure was followed on day 7 to deliver VEGF for a second round. Wounds were inspected every 2 days and the bandage was changed and a picture of the wound was taken using a digital camera. On day 19, all animals were sacrificed using 20% CO2 volume displacement (flow rate cage volume/per min) anesthetic overdose and wound tissue was harvested and fixed using 4% paraformaldehyde (PFA).

Histology:

Frozen sections of haired skin were stored in a −80 °C ultralow freezer prior to sectioning on a cryotome. The sections of skin were cut 10 μm thick using a Thermo Scientific CryoStar NX50, routinely stained with hematoxylin and eosin on a Leica ST5020 H&E stainer, and coverslipped with a Leica CV5030 coverslipper. A veterinary anatomic pathologist who is board certified by the American College of Veterinary Pathologists performed all histological evaluations.

Immunohistochemistry Staining:

PFA-fixed and optimal cutting temperature compound-embedded biopsy sections of the full thickness skin were cut into 10 μm thick samples using a Thermo Scientific CryoStar NX50. Slides were washed and immunofluorescence staining was performed for assessment of vascularization and inflammation in harvested skin from the animal study. A heat-induced antigen retrieval protocol followed for immunofluorescence immunohistochemistry (IF/IHC). Slides were heated in an oven and washed multiple times with xylene and alcohol with automated device (HistoCore SPECTRA ST) then heated in 100 °C sodium citrate buffer (10×10^{-3}M sodium citrate, 0.05% Tween 20, pH 6.0) for 20 min for antigen retrieval and were permeabilized in 0.5% v/v Triton for 20 min. Skin sections were then blocked with 5% BSA (30 min) and 5% goat serum (30 min). The CD31 and MMP-9 primary antibodies were diluted at a ratio of 1:50 and 1:200, respectively, and stained the skin sections overnight at −20 °C. Then, the secondary antibodies were diluted at a ratio of 1:200 and stained the skin samples for 2 h for visualization. Slides were mounted with mounting solution (Glycerol Tris Buffer PH 9.0) and coverslipped and imaged with a Zeiss fluorescent microscope.

Supplementary Material

Refer to Web version on PubMed Central for supplementary material.

Acknowledgements

The financial support from the National Institutes of Health (GM126831, AR073822, and P20GM113126), the National Science Foundation (Award No. 1826135), the University of Nebraska-Lincoln, and Nebraska Tobacco Settlement Biomedical Research Enhancement Funds are gratefully acknowledged. The authors also gratefully thank Carina Russel, Jacob Quint, Kristen Reynolds and Morgan Schake for their assistance throughout the project.

References

[1]. Frykberg RG, Banks J, Adv. Wound Care 2015, 4, 560.

[2]. a) Werdin F, Tenenhaus M, Rennekampff H-OJTL, Lancet 2008, 372, 1860; [PubMed: 19041788] b) Lindholm C, Searle R, Int. Wound J 2016, 13, 5.

[3]. a) Sen CK, Gordillo GM, Roy S, Kirsner R, Lambert L, Hunt TK, Gottrup F, Gurtner GC, Longaker MT, Wound Repair Regener. 2009, 17, 763;b) Fife CE, Carter MJ, Wounds 2012, 24, 10. [PubMed: 25875947]

[4]. a) Guo S, DiPietro LA, J. Dent. Res 2010, 89, 219; [PubMed: 20139336] b) Saghazadeh S, Rinoldi C, Schot M, Kashaf SS, Sharifi F, Jalilian E, Nuutila K, Giatsidis G, Mostafalu P, Derakhshandeh H, Yue K, Swieszkowski W, Memic A, Tamayol A, Khademhosseini A, Adv. Drug Delivery Rev 2018, 127, 138;c) Guo J, Dardik A, Fang K, Huang R, Gu Y, Stem Cell Res. Ther 2017, 8, 228. [PubMed: 29037219]

[5]. a) Demidova-Rice TN, Hamblin MR, Herman IM, Adv. Skin Wound Care 2012, 25, 304; [PubMed: 22713781] b) Percival, McCarty SM, Lipsky B, Adv. Wound Care 2015, 4, 373.

[6]. Mustoe TA, O'Shaughnessy K, Kloeters O, Plast. Reconstr. Surg 2006, 117, 35S. [PubMed: 16799373]

[7]. Tamayol A, Hassani Najafabadi A, Mostafalu P, Yetisen AK, Commotto M, Aldhahri M, Abdel-wahab MS, Najafabadi ZI, Latifi S, Akbari M, Annabi N, Yun SH, Memic A, Dokmeci MR, Khademhosseini A, Sci. Rep 2017, 7, 9220. [PubMed: 28835675]

[8]. Pop MA, Almquist BD, Exp. Dermatol 2017, 26, 760. [PubMed: 28094868]

[9]. Yamakawa S, Hayashida K, Burns Trauma 2019, 7, 10. [PubMed: 30993143]

[10]. Derakhshandeh H, Kashaf SS, Aghabaglou F, Ghanavati IO, Tamayol A, Trends Biotechnol. 2018, 36, 1259. [PubMed: 30197225]

[11]. Bagherifard S, Tamayol A, Mostafalu P, Akbari M, Comotto M, Annabi N, Ghaderi M, Sonkusale S, Dokmeci MR, Khademhosseini A, Adv. Healthcare Mater 2016, 5, 175.

[12]. a) Kiaee G, Mostafalu P, Samandari M, Sonkusale S, Adv. Healthcare Mater 2018, 7, 1800396;b) Mostafalu P, Kiaee G, Giatsidis G, Khalilpour A, Nabavinia M, Dokmeci MR, Sonkusale S, Orgill DP, Tamayol A, Khademhosseini A, Adv. Funct. Mater 2017, 27, 1702399;c) Tamayol A, Akbari M, Zilberman Y, Comotto M, Lesha E, Serex L, Bagherifard S, Chen Y, Fu G, Ameri SK, Ruan W, Miller EL, Dokmeci MR, Sonkusale S, Khademhosseini A, Adv. Healthcare Mater 2016, 5, 711;d) Boateng J, Catanzano O, J. Pharm. Sci 2015, 104, 3653. [PubMed: 26308473]

[13]. Punjiya M, Mostafalu P, Sonkusale S, presented at 2017 IEEE 60th International Midwest Symposium on Circuits and Systems (MWSCAS), Medford, MA, August 2017.

[14]. Fair RJ, Tor Y, Perspect. Medicin. Chem 2014, 6, 25. [PubMed: 25232278]

[15]. Mostafalu P, Tamayol A, Rahimi R, Ochoa M, Khalilpour A, Kiaee G, Yazdi IK, Bagherifard S, Dokmeci MR, Ziaie B, Sonkusale SR, Khademhosseini A, Small 2018, 14, 1870150.

[16]. van der Maaden K, Jiskoot W, Bouwstra J, J. Controlled Release 2012, 161, 645.

[17]. Farzin A, Miri AK, Sharifi F, Faramarzi N, Jaberi A, Mostafavi A, Solorzano R, Zhang YS, Annabi N, Khademhosseini A, Tamayol A, Adv. Healthcare Mater 2018, 7, 1800702.

[18]. Lee Y, Hwang K, Surg. Radiol. Anat 2002, 24, 183. [PubMed: 12375070]

[19]. a) Rinkel WD, Rizopoulos D, Aziz MH, Van Neck JW, Cabezas MC, Coert JH, Muscle Nerve 2018, 58, 559; [PubMed: 30028522] b) Ahmad J, Diabetes Metab. Syndr.: Clin. Res. Rev 2016, 10, 48.

[20]. Rimington RP, Capel AJ, Player DJ, Bibb RJ, Christie SDR, Lewis MP, Macromol. Biosci 2018, 18, 1800113.

[21]. Mata A, Fleischman AJ, Roy S, Biomed. Microdevices 2005, 7, 281. [PubMed: 16404506]

[22]. Zhang D, Das DB, Rielly CD, J. Pharm. Sci 2014, 103, 613. [PubMed: 24399616]

[23]. Coleman DL, Diabetologia 1978, 14, 141. [PubMed: 350680]

[24]. a) Kunugiza Y, Tomita N, Taniyama Y, Tomita T, Osako MK, Tamai K, Tanabe T, Kaneda Y, Yoshikawa H, Morishita R, Gene Ther. 2006, 13, 1143; [PubMed: 16572191] b) Sudheesh Kumar PT, Lakshmanan V-K, Anilkumar TV, Ramya C, Reshmi P, Unnikrishnan AG, Nair SV, Jayakumar R, ACS Appl. Mater. Interfaces 2012, 4, 2618; [PubMed: 22489770] c) Choi JS, Leong KW, Yoo HS, Biomaterials 2008, 29, 587; [PubMed: 17997153] d) Randeria PS, Seeger MA, Wang X-Q, Wilson H, Shipp D, Mirkin CA, Paller AS, Proc. Natl. Acad. Sci. USA 2015, 112, 5573. [PubMed: 25902507]

[25]. Yano K, Brown LF, Detmar M, J. Clin. Invest 2001, 107, 409. [PubMed: 11181640]

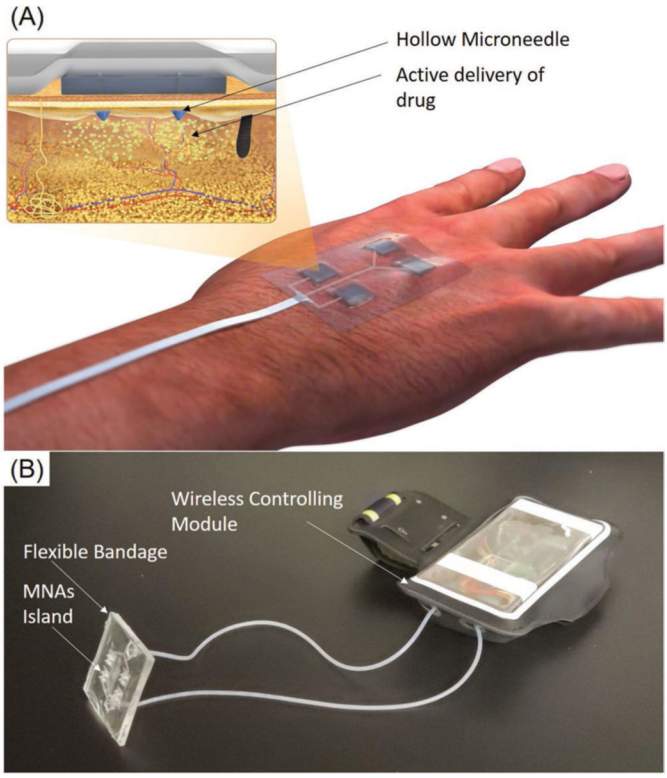

Figure 1.

The wirelessly controlled smart bandage equipped with MNAs for delivery of therapeutics. A) Schematic of the engineered bandage and its operation. B) A representative photograph of the bandages for the delivery of multiple drugs. The system had two modules, a wearable bandage with integrated MNAs connected to the controlling module, which can communicate wirelessly with a smartphone in order to control the drug delivery rate.

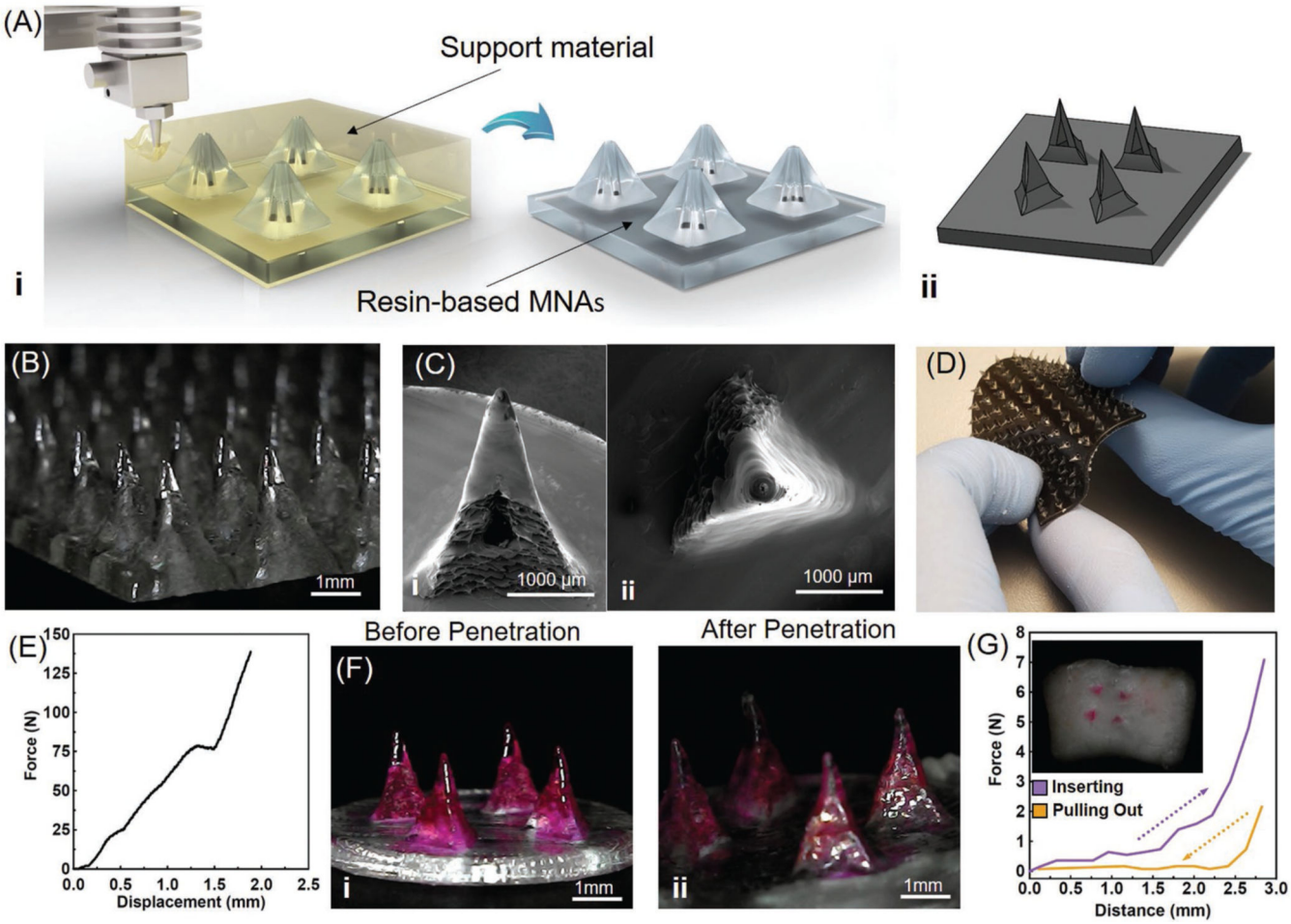

Figure 2.

Fabrication and characterization of 3D-printed MNAs. A) Schematic of 3D-printing MNAs showing i) the fabrication process and ii) a representative computer model view of the designed hollow MNAs. B) Microscopic image of sample MNAs. C) SEM images of i) front view and ii) top view of a single hollow needle. D) Multimaterial printing of MNAs for creating rigid needles on a flexible base. E) The characterization of the mechanical properties of MNA islands (four needles) ($n = 4$). F) Microscopic view of MNAs i) before and ii) after pig skin penetration test ($n = 4$). G) Characterization of the insertion and pull out force of the MNA islands applied to pig skin and image of pig skin targeted with painted MNAs (inset).

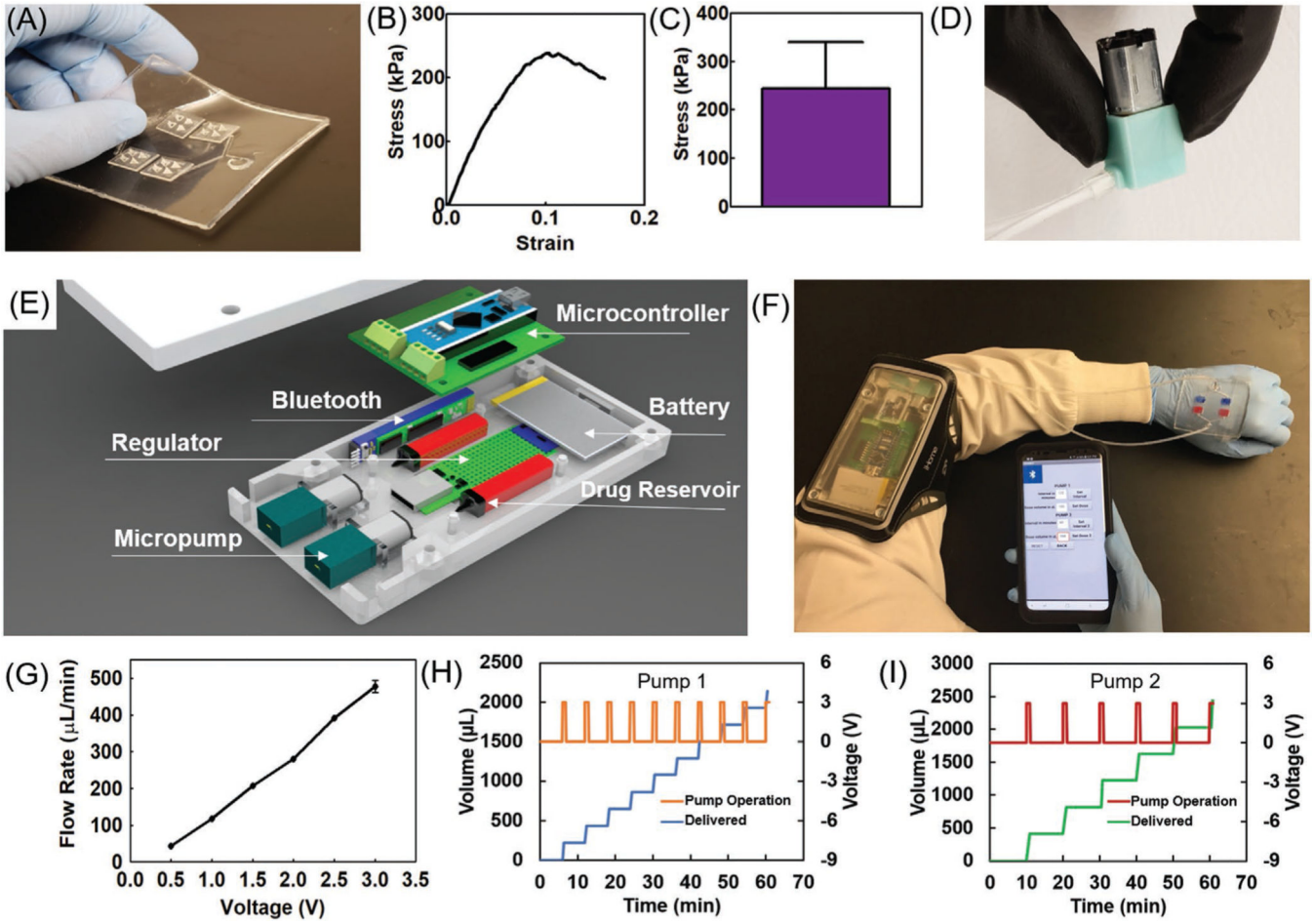

Figure 3.

Characterization of microcontroller and wireless software. A) Photograph of a typical fabricated flexible bandage with bonded hollow MNAs on a PDMS-made bandage. B) A representative stress-strain curve of a peel-off test for assessment of the bonding strength of resin to PDMS. C) The bonding strength of resin and PDMS substrates ($n = 6$). D) Photograph of the micropump used for the drug delivery system. E) Schematic view of the microcontroller and its components. F) Example of the integrated system operation on the human body. G) Calibration plot of the micropump flow rate as a function of applied voltage ($n = 3$). H,I) The cumulative delivered solution using two independent pumps on a single bandage subjected to different periodic functions of applied voltage calibrated to produce a flow rate of 200 μL every 6 min for pump 1 and 400 μL every 10 min for pump 2 ($n = 3$ for each pump).

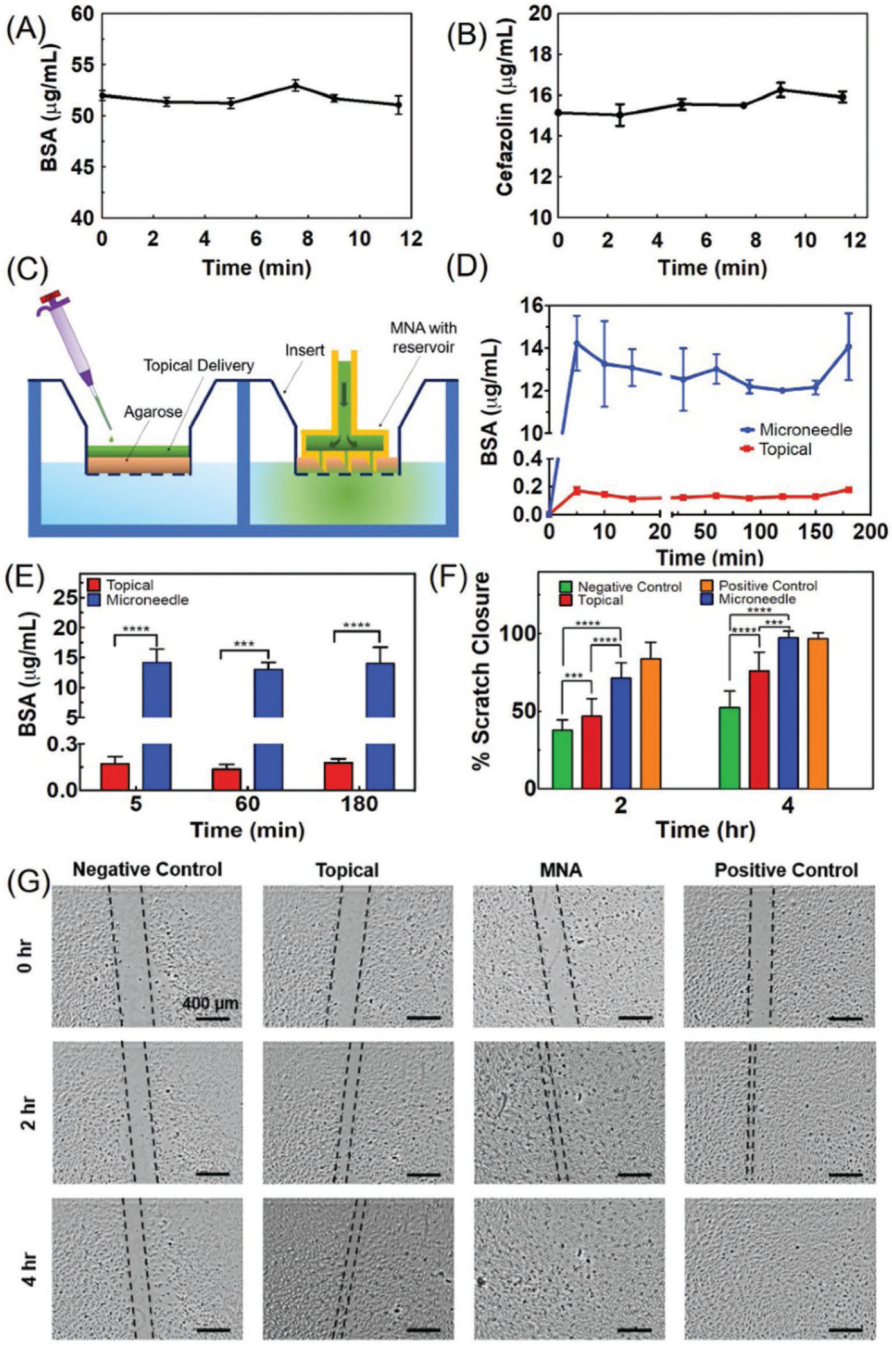

Figure 4.

Characterizing the drug release and its effect on cellular cultures. A,B) The concentration of BSA and cefazolin in solutions perfused through the engineered bandage and MNAs over time. The results suggest an insignificant change in concentration ($n = 3$ for each solution). C) Schematic of the two-compartment in vitro model used for simulating chronic wounds covered by a crust and necrotic tissue used for comparing the topical and MNA-based drug delivery. D) The cumulative concentration of the BSA in the bottom chamber representing the wound bed after the administration of 20 μg mL^{-1} solution of BSA through 2 mm thick

agarose gel (3% w/v) within a cell culture insert ($n = 3$ for each group). E) The cumulative drug concentration after 5, 60, and 180 min postdrug administration (***$P < 0.001$, ****$P < 0.0001$). F,G) Scratch assay on the culture of HUVECs receiving the following treatments: 1) 50 ng mL^{-1} of VEGF in the culture medium (positive control), 2) no VEGF (negative control), 3) equivalent to 50 ng mL^{-1} delivered topically, and 4) equivalent to 50 ng mL^{-1} delivered using the MNAs ($n = 5$ for each group) (***$P < 0.001$, ****$P < 0.0001$). Representative micrographs are shown in (G).

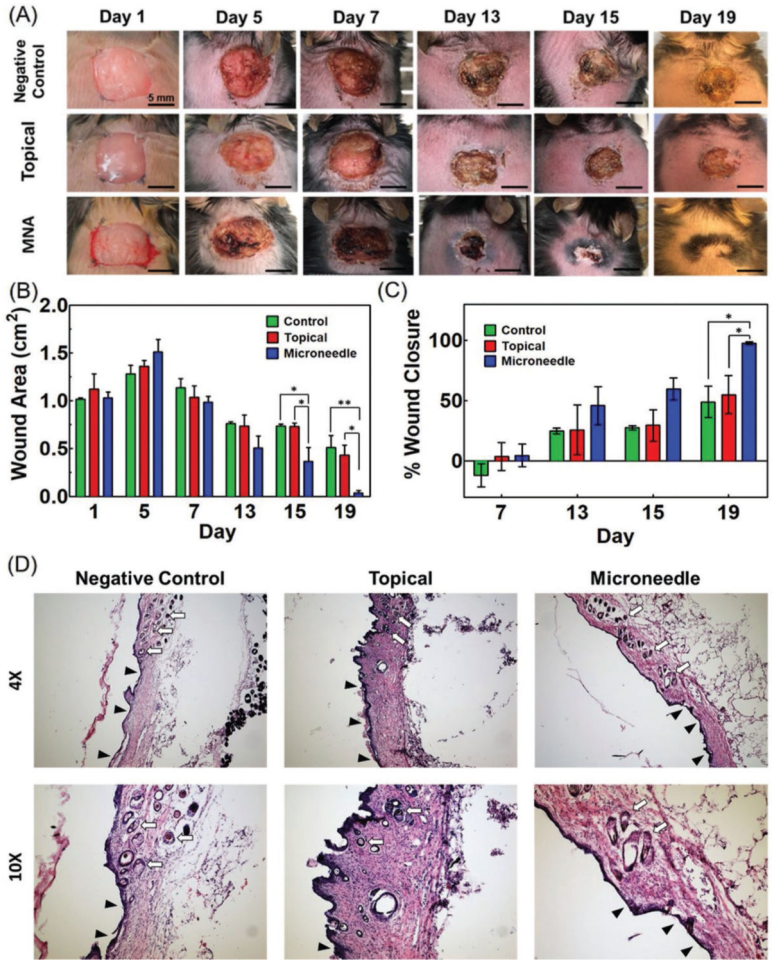

Figure 5.

Animal studies for assessment of the effectiveness of VEGF delivery through MNAs on diabetic wound healing. Full thickness wounds (1 cm × 1 cm) were formed on the dorsum of diabetic mice. A) Representative images showing wound healing progression in three mice groups (control (no VEGF) ($n = 4$), topically applied VEGF ($n = 4$), and MNA-based VEGF delivery ($n = 5$)) over 19 days. B,C) Significant wound closure (95%) was observed in MNA-based VEGF delivery group while no treatment and topical delivery groups showed an average healing rate of 40% and 50%, respectively (*$P < 0.05$, **$P < 0.01$). Wound closure rate was calculated as the ratio (percentage) of the open wound area at each measured time point divided by the area of the wound at time 0 (day 1). D) H&E staining for characterization of granulation tissue and neovascularization as well as hair growth in the skin in all three study groups is shown in two different magnifications. The ulcers with an underlying bed of granulation tissue are denoted with black arrowheads and hair growth is denoted with white arrows.